International Journal of Chemical, Materials and Biomolecular Sciences
ISSN: 2415-6620
Vol:11, No:5, 2017

Annealing of the Contact between Graphene and Metal: Electrical and Raman Study

A. Sakavičius, A. Lukša, V. Nargelienė, V. Bukauskas, G. Astromskas, A. Šetkus

***Abstract*—**We investigate the influence of annealing on the properties of a contact between graphene and metal (Au and Ni), using circular transmission line model (CTLM) contact geometry. Kelvin probe force microscopy (KPFM) and Raman spectroscopy are applied for characterization of the surface and interface properties. Annealing causes a decrease of the metal-graphene contact resistance for both Ni and Au.

***Keywords*—**Graphene, Kelvin force probe microscopy, Raman spectroscopy.

I. Introduction

IN the last few years, various electronic applications for graphene monolayers, exploiting their electrical, optical and wide functional properties, were proposed [1]-[6]. Chemical vapor deposition (CVD) grown graphene remains material of choice for device fabrication due to promising electrical properties and scalability for industrial fabrication [7], [8]. However, the bottle-neck for the applications is high electrical resistance of the graphene/metal contacts. In addition, an interaction between graphene and metal significantly modifies electrical properties of graphene [9], [10].

In this work, we investigate two types of the contacts; namely Au and Ni, known to be physisorbed and chemisorbed with graphene. We study the influence of annealing on the electrical parameters – contact resistance and sheet resistance using CTLM geometry. In parallel, we investigate the variations in the Raman spectra and the work function of the surface. As we wet-transfer graphene layer on top of CTLM patterns made of whether Au or Ni, the "top transfer" strategy allows us to measure the effect of annealing with Raman and KPFM on the same contacts. We anneal graphene on top of metal contact at 300 °C in Ar for up to 2h in successive steps. We then are able to directly relate the annealing induced changes in the electrical resistance to the shifts of the Raman peaks and changes in the metal work function, without the need of additional processing steps to remove metal layers [11].

II. Materials and Methods

We start by forming CTLM structures on SiO_2/Si substrate with optical lithography, using AZ5214E resist. The diameter of inner CTLM contact is 100 µm. The distance between inner and outer contacts varies from 5 to 30 µm. We then sputter Au or Ni layers – 100 nm for Au and 80 nm for Ni and perform liftoff in AZ 100 remover. CVD monolayer graphene (from Graphenea S. A.) film deposited on Cu substrate is wet-transferred on SiO_2/Si substrate using Acros Organics M. W. 35000 PMMA (polymethyl-methacrylate) polymer, using a standard recipe [12]. First, we spincoat PMMA layer and dry the samples at 150 °C temperature for 30 min. Then, we etch Cu substrate with $HCl:H_2O_2:H_2O$ (5:2:30) solution for up to 20 min. We rinse the graphene/PMMA structure in DI water for 3 x20 minutes and dip the substrate with CTLM pattern to transfer graphene layer. Afterwards, PMMA is dissolved in chloroform for 15 hours and rinsed with IPA. Graphene layer transferred on metal contacts is illustrated in Fig. 1. The full sample composition is as follows: Si/SiO_2/Metal/Graphene. Hence, in this article we use shorter abbreviation of the sample structure – Metal/Graphene.

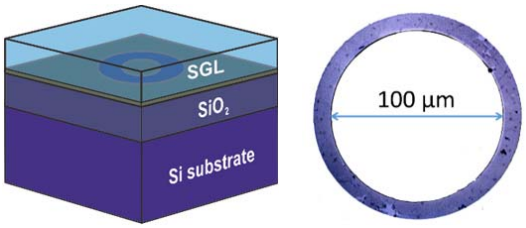

(a) (b)

Fig. 1 Graphene transferred on metal contacts (a) Sketch of single layer graphene (SGL) transfer from Cu substrate to already formed CTLM structure; (b) Optical image of graphene laying on CTLM structure; SiO_2 patterns in contact area allow to identify wrinkles and cracked graphene regions

After the wet-transfer, we measure electrical, Raman and Kelvin characteristics, noting which particular structure is measured. We then anneal samples at 300 °C in Ar (purity >=99.999%) using RTP-100-HW rapid thermal annealing furnace, under 2 slm flow at ambient pressure. We flow 2 slm Ar at ambient pressure. Cumulative annealing time is 124 min, consisting of 4 min, 60 min, and 60 min successive durations. After particular annealing step, electrical properties and Raman spectra are measured on the same structure.

Electrical measurements are performed on Cascade Microtech Summit 11000/12000 probe station, using Keithley 4200SCS parameter analyzer. Raman spectra are recorded using Renishaw inVia spectrometer, using 633 nm (1.96 eV) laser at 0.79 mW power. Raman scattering wavenumber axis

A. Sakavičius is with the National Centre of Physical and Technological Sciences, Vilnius, LT-10257 Lithuania (phone: +370-5262-7937; fax: +370-5260-2317; e-mail: andrius.sakavicius@ftmc.lt).

A. Lukša, V. Nargelienė, V. Bukauskas, G. Astromskas, ans A. Šetkus are with the National Centre of Physical and Technological Sciences, Vilnius, LT-10257 Lithuania (e-mail: algimantas.luksa@ftmc.lt, viktorija.nargeliene@ftmc.lt, virginijus.bukauskas@ftmc.lt, astromskas@ftmc.lt, arunas.setkus@ftmc.lt).

was calibrated by the silicon peak at 520.7 nm. The 50x/0.75 objective is used to focus the spot within an individual CTLM contact. Raman spectra peak positions and Full Width at Half Maximum (FWHM) are extracted from fitted Lorentzian shape components. Raman spectra are measured at each sample for 5 times.

Kelvin probe measurements are done using NanoScope Dimension 3100 IVa AFM setup. Measurements were calibrated on HOPG substrate.

A. Electrical Measurements

In Fig. 2, we show the measured CTLM resistance of different devices for Ni (Fig. 2 (a)) and Au contacts (Fig. 2 (b)). We observe that the resistance decreases after 4 min annealing for all measured devices proportionally to particular structures initial resistances. Therefore, the error bars in the CTLM analysis, shown in Fig. 3, are not directly related to statistical fluctuations, but are caused by a particular arrangement of multicrystalline CVD graphene. The resistance decreases for all annealing times, but the main reduction occurs after initial 4 minutes annealing.

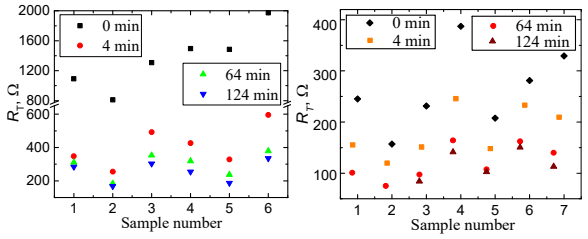

(a) (b)

Fig. 2 Comparison of the measured resistances of CTLM structures with 30 µm distance between metal contacts before (0 min) and after 4, 64, and 124 min annealing (a) Ni/Graphene; (b) Au/Graphene

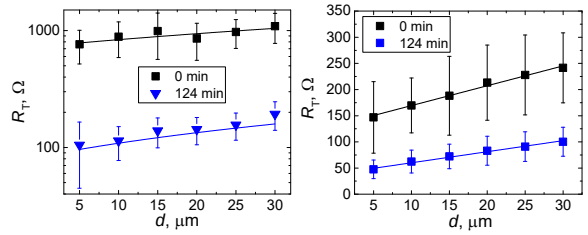

(a) (b)

Fig. 3 CTLM resistance versus distance plots for (a) Ni and (b) Au contacts. Total device resistance R_T dependence on distance between contacts d before annealing (black curve) and after 124 min annealing (blue curve)

Fig. 3 shows the measured resistances of CTLM structures at different annealing times Ni and Au CTLM patterns. The measured resistances rapidly reduce after 4 min annealing as compared to freshly transferred graphene sample, but in Fig. 3, we demonstrate total device resistance dependence on distance between metal contacts just before annealing and after 124 min annealing. However, the large distribution of the measured resistances is observed, similar to the reported results by Politou et al. [13]. This is attributed to the multicrystalline structure of the monolayer CVD graphene. The total measured resistance is higher for Ni contacts than for Au contacts both before and after annealing. Raman measurements of evaporated Ni show carbide free Ni, while annealing induces NiC formation. This can explain the difference in the contact resistance between Au and Ni. The annealing also decreases sheet resistance of graphene using either metal, but it is less than the contact resistance. This indicates that annealing affects the contact area as well as graphene layer.

In Fig. 4, we show extracted contact and sheet resistances of Au, Ni contacts to graphene. We observe that R_C of Au/ Graphene devices reduces from 20.5 kΩµm to 6.1 kΩµm after 2 h thermal annealing. R_C of Ni/Graphene reduces from 114.9 kΩµm to 13.3 Ωµm after 2h thermal annealing. We also manufactured NiC contacts to verify the effect of NiC formation on observed resistances on Ni structures. For NiC/Graphene, a 60-minute annealing reduces R_C from 327.5 kΩµm to 8.1 Ωµm. Meanwhile, R_{Sh} does not show large reduction for Au contact (from 1.2 kΩ/□ to 0.6 kΩ/□) indicating that annealing mainly improves Au/Graphene contacts without affecting graphene layer. The sheet resistance on Ni contacts lowers from 3.3 kΩ/□ to 0.9 kΩ/□ after 2h annealing. The most rapid reduction of R_{Sh} for both Ni/Graphene and Au/Graphene contacts is observed after 4 minutes annealing, while subsequent annealing exhibits near saturation of sheet resistance. R_{Sh} of NiC/Graphene devices reduces from 5.4 kΩ/□ to 3.1 kΩ/□ after 60 minutes annealing, higher than for Ni contacts.

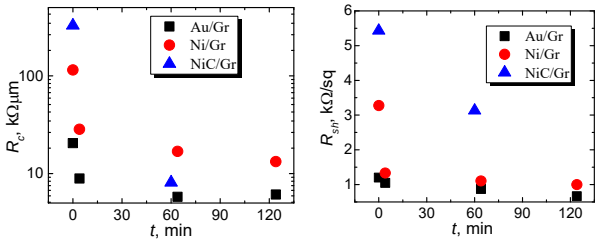

(a) (b)

Fig. 4 Average contact resistance <R_C> (a) and average sheet resistance <R_{Sh}> (b) dependencies on rapid thermal annealing time (t_{anneal}) of Au/Graphene and Ni/Graphene contacts: each data point consists of more than 25 experimental values

The manner of changes of contact and sheet resistance is very similar even after different annealing steps, making it difficult to separate how annealing affects each of these resistances. Therefore, we have chosen to selectively analyze structures, deciding on six samples which have lowest resistance and six samples with the highest resistance for each inter-contact distance of the CTLM dataset. We expect high resistance samples to be dominated only by the contact resistance, while low resistance samples to have a combination of both of sheet resistance and contact resistance in the CTLM analysis. First, we analyze Au samples, (shown in Fig. 5 (a)),

where initial R_C (no annealing) is almost four times lower for samples, having low individual resistance, as compared to samples with high resistance. However, 4-min annealing makes contact resistances of both sets similar. This is not affected even by the subsequent 2 h annealing. We propose that contact resistance of large resistance structures changes due to annealing induced reduction of distance between metal and graphene [14]. The subsequent annealing induces further reduction, therefore leading to constant contact resistance, and no alloy formation between Au and graphene is expected.

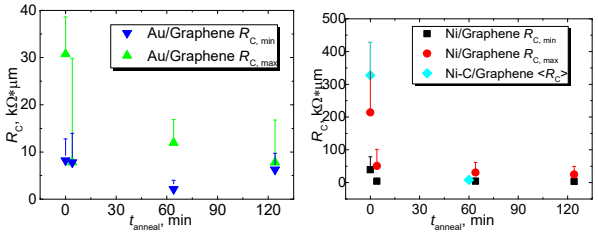

(a) (b)

Fig. 5 Variation of R_C of Metal/Graphene devices versus annealing time (a) R_C derived from six samples of the lowest and highest resistance of Au/Graphene devices; (b) R_C derived from six samples of the lowest and highest resistance of Ni/Graphene devices and average resistance of NiC/Graphene devices

For Ni samples (shown in Fig. 5 (b), a similar dependence is observed. Resistance of samples is prevailed by contact resistance. The annealing reduces contact resistance for both structures, but the change is larger for high resistance samples. However, the small change observed for low resistance structures is within the error bars. Therefore, we propose that contact resistance on Ni structures reduces due to annealing induced reduction of distance between metal and graphene layer as well. This is further supported by the fact that NiC structures also show lowering of contact resistance after annealing, opposing the idea of continuous barrier formation between graphene and NiC.

III. Raman Spectroscopy

The change of electrical resistance is related to a change of the metal-graphene interface [15], [16]. Therefore, we measured Raman spectra of the samples before and after annealing to distinguish the mechanism of the annealing induced contact resistance improvement. Raman spectroscopy is a nondestructive tool to characterize graphene doping, edges, strain and stress, disorder [6], [15], [16].

The shift of G and 2D peaks is sensitive to doping and/or stress of graphene layer. We observe that 2D peak demonstrates the blue-shift shift after annealing.

The shifts of G and 2D peaks are related to mainly to stress and doping of the graphene layer. In our case, we can measure these shifts on both metal/graphene contact, as well as SiO_2/graphene surface of the same device, to separate annealing induced changes in contact and graphene layer. However, we do not observe considerable G peak shift after anneal. According to Raman spectra, graphene on SiO_2 substrate does not exhibit difference whether it was transferred on Au (Fig. 7 (a) or Ni (Fig. 7 (b)) sample. Even after annealing, positions of G and 2D peaks are almost the same. On the contrary, we observe huge difference of 2D peak positions if we compare graphene transferred on different metal contacts.

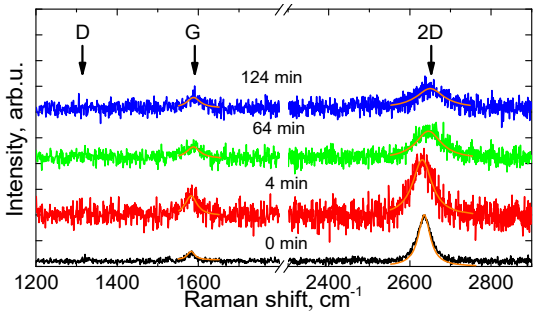

Fig. 6 Raman spectra versus annealing time: Raman spectra obtained of one Graphene on Nickel/Graphene device; orange curve shows fitting of peak curves using Lorentzian peaks

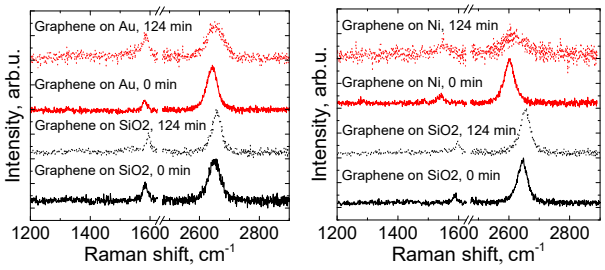

(a) (b)

Fig. 7 Raman spectra of graphene transferred on SiO_2 substrate and metal contacts before annealing (solid line) and after 2h annealing (dots); (a) Raman spectra of graphene transferred on SiO_2 substrate and Au contacts (b) Raman spectra of graphene transferred on SiO_2 substrate and Ni contacts

A more interesting situation occurs when analyzing 2D peak shift of graphene transferred on metal contacts (Fig. 8). 2D peak of graphene of Au/Graphene and Ni/Graphene structures is blue-shifted by different amount after 64-min annealing.. This indicates that annealing induced doping of the graphene is not due to PMMA process used, but due to metal contact under the graphene layer. Both Ni and Au induce doping into the graphene layer, but albeit at different quantities.

It is known that 2D peak blue-shifting is related to the Fermi level in graphene, and we attribute the shift to the doping by holes, as reported for PMMA based wet transfer process [17]. Moreover, blue shift of 2D peak could be related to reduction of stress between graphene and substrate [18]. We also measured 2D peak shifts on NiC/Graphene contact, as the NiC formation is known to cause an increase of graphene contact resistance. The NiC causes a 2D peak red-shift, while 2D peak of NiC on SiO_2 surface is blue shifted. The shift of 2D peak to lower energies indicates n-type induced doping

[19]. According to the 2D peak shift of graphene on Ni contacts, we observe n-type doping after 4 min annealing. After further annealing steps, type of doping is similar to NiC samples. We expect that additional annealing of PMMA transferred samples suppresses n-type contact induced doping to favor the PMMA induced p-type. FWHM of G and 2D of graphene on Au and Ni contacts increases with annealing time. It is known that increase of FWHM of G peak could be related with disorder in graphene layer [16].

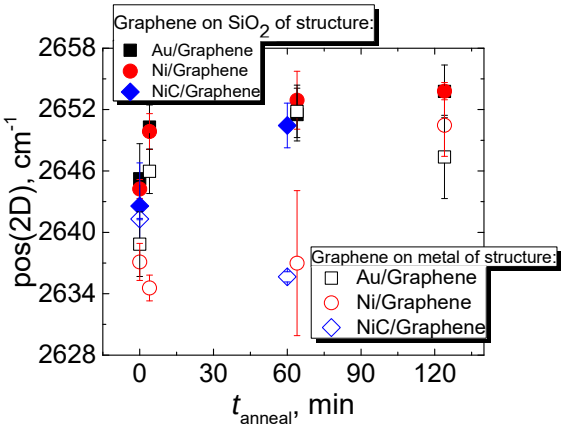

Fig. 8 Raman shift of 2D peak position versus anneal time: solid symbol represents graphene on SiO_2 (between Au (black), Ni (red) and NiC (blue) metal contacts). Unfilled symbol represents Au/Graphene (black), Ni/Graphene (red) and NiC/Graphene (blue) metal contacts

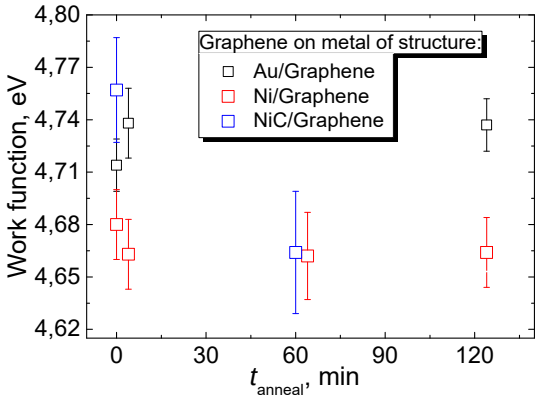

Fig. 9 Work function versus annealing time of following structures: Au/Graphene (unfilled black dots), Ni/Graphene (unfilled red dots), NiC/Graphene structure (unfilled blue dots)

IV. Kelvin Force Probe Measurements

Kelvin Force Probe Microscopy (KPFM) evaluates the doping type of metal/graphene contact [20]-[21]. KFPM in our experiment shows an increase of the electron work function after annealing of graphene on Au contacts, as shown in (Fig. 9 black dots). This indicates the increased p-doping of the Au/Graphene system. Work function increases at SiO_2/Graphene area for Au/Graphene device as well, as expected for graphene samples, transferred with PMMA. The p-doping agrees with Raman spectroscopy measurements. Furthermore, we observe that work function of Au/Graphene devices reaches the 4.7 eV value. This leads to formation of 3.7 Å distance between Au and graphene [14], [22]. The value of work function remains almost the same with the increase of the annealing time and close to the theoretical value of the work function separation between Au and graphene [23].

V. Conclusion

The annealing results in significant reduction of the contact resistance for the tested Au/Graphene, Ni/Graphene, and NiC/Graphene structures. We propose that contact resistance decreases mainly due to reduction of distance between metal contact and graphene layer for Au/Graphene, Ni/Graphene, and NiC/Graphene, while higher contact resistance for Ni/Graphene and NiC/Graphene contacts, compared to Au/Graphene, is attributed to NiC formation during the annealing.

We measure the 2D peak shift for graphene on the SiO_2 in all tested samples. Taking into account that the 2D peak shift can be related to the Fermi level in graphene, a p-type doping is supposed to be in the graphene layer due to surface charges at SiO_2/graphene interface and due to PMMA residues. When comparing graphene on top of metal structures, we observe 2D peak shifts in different direction for Ni and Au. The Au/Graphene interface is even more shifted towards p-type, while Ni layer induces nearly no shift of the 2D peak. These results indicate that mechanism for contact resistance decrease is different between the two metals. The NiC causes a 2D peak shift towards lower wavenumbers, indicating an n-type induced doping. Considering similar shift for the Ni/Graphene contact, we propose that the properties of the contact between Ni and graphene are dependent on the formation of NiC. KFPM shows an increase of the work function after the annealing for Au/Graphene contacts, as expected for p-type doped graphene.

References

[1] Novoselov, Kostya S., et al. "Electric field effect in atomically thin carbon films." Science 306.5696 (2004): 666-669.
[2] Novoselov, Kostya S., et al. "Two-dimensional gas of massless Dirac fermions in graphene." Nature 438.7065 (2005): 197-200.
[3] Novoselov, K. S., et al. "Two-dimensional atomic crystals." Proceedings of the National Academy of Sciences of the United States of America 102.30 (2005): 10451-10453.
[4] Geim, Andre K., and Konstantin S. Novoselov. "The rise of graphene." Nature materials 6.3 (2007): 183-191.
[5] Stankovich, Sasha, et al. "Graphene-based composite materials." Nature 442.7100 (2006): 282-286.
[6] Ferrari, A. C., et al. "Raman spectrum of graphene and graphene layers." Physical review letters 97.18 (2006): 187401.
[7] Kang, Junmo, et al. "Graphene transfer: key for applications." Nanoscale 4.18 (2012): 5527-5537.
[8] Neto, AH Castro, et al. "The electronic properties of graphene." Reviews of modern physics 81.1 (2009): 109.
[9] Venugopal, A., L. Colombo, and E. M. Vogel. "Contact resistance in few and multilayer graphene devices." Applied Physics Letters 96.1 (2010): 013512.
[10] Li, Wei, et al. "Ultraviolet/ozone treatment to reduce metal-graphene contact resistance." Applied Physics Letters 102.18 (2013): 183110.
[11] Leong, Wei Sun, Chang Tai Nai, and John TL Thong. "What does annealing do to metal–graphene contacts?." Nano letters 14.7 (2014):

3840-3847.
[12] Liang, Xuelei, et al. "Toward clean and crackless transfer of graphene." ACS nano 5.11 (2011): 9144-9153.
[13] Politou, Maria, et al. "Transition metal contacts to graphene." Applied Physics Letters 107.15 (2015): 153104.
[14] Matsuda, Yuki, Wei-Qiao Deng, and William A. Goddard III. "Contact Resistance for "End-Contacted" Metal− Graphene and Metal− Nanotube Interfaces from Quantum Mechanics." The Journal of Physical Chemistry C 114.41 (2010): 17845-17850.
[15] Das, Anindya, et al. "Monitoring dopants by Raman scattering in an electrochemically top-gated graphene transistor." Nature Nanotechnology 3.4 (2008): 210-215.
[16] Ferrari, Andrea C., and Denis M. Basko. "Raman spectroscopy as a versatile tool for studying the properties of graphene." Nature Nanotechnology 8.4 (2013): 235-246.
[17] Cheng, Zengguang, et al. "Toward intrinsic graphene surfaces: a systematic study on thermal annealing and wet-chemical treatment of SiO2-supported graphene devices." Nano letters 11.2 (2011): 767-771.
[18] Ni, Zhen Hua, et al. "Uniaxial strain on graphene: Raman spectroscopy study and band-gap opening." ACS nano 2.11 (2008): 2301-2305.
[19] Wang, W. X., et al. "The study of interaction between graphene and metals by Raman spectroscopy." Journal of Applied Physics 109.7 (2011): 07C501.
[20] Ziegler, D., et al. "Variations in the work function of doped single-and few-layer graphene assessed by Kelvin probe force microscopy and density functional theory." Physical Review B 83.23 (2011): 235434.
[21] Yu, Young-Jun, et al. "Tuning the graphene work function by electric field effect." Nano letters 9.10 (2009): 3430-3434.
[22] Giovannetti, G. A. K. P. A., et al. "Doping graphene with metal contacts." Physical Review Letters 101.2 (2008): 026803.
[23] Khomyakov, P. A., et al. "First-principles study of the interaction and charge transfer between graphene and metals." Physical Review B 79.19 (2009): 195425.